

# Flexible and efficient discretizations of multilayer models with variable density

Luca Bonaventura <sup>(1)</sup> and José Garres-Díaz <sup>(2)</sup>

July 28, 2020

<sup>(1)</sup> MOX – Modelling and Scientific Computing,  
Dipartimento di Matematica, Politecnico di Milano  
Via Bonardi 9, 20133 Milano, Italy  
`luca.bonaventura@polimi.it`

<sup>(2)</sup> Departamento de Matemáticas, Universidad de Córdoba  
Campus de Rabanales, 14014, Córdoba, Spain  
`jgarres@uco.es`

**Keywords:** Semi-implicit method, multilayer approach, depth-averaged model, mass exchange, stratified flow.

**AMS Subject Classification:** 35F31, 35L04, 65M06, 65N08, 76D33

## Abstract

We show that the semi-implicit time discretization approaches previously introduced for multilayer shallow water models for the barotropic case can be also applied to the variable density case with Boussinesq approximation. Furthermore, also for the variable density equations, a variable number of layers can be used, so as to achieve greater flexibility and efficiency of the resulting multilayer approach. An analysis of the linearized system, which allows to derive linear stability parameters in simple configurations, and the resulting spatially semi-discretized equations are presented. A number of numerical experiments demonstrate the effectiveness of the proposed approach.

## 1 Introduction

Multilayer shallow water models [1, 3, 2, 4] have become quite popular in the last two decades to reduce the computational cost of river and coastal flow simulations. A version of these models was derived in [8] from the full Navier-Stokes system, by assuming a discontinuous profile of velocity, showing that the solution of the multilayer model is a particular weak solution of the full Navier-Stokes system. In our previous work [5], we have shown that, in the barotropic, constant density and hydrostatic case, these models can be made more computationally efficient by two complementary strategies. On the one hand, a classical semi-implicit time discretization can be employed to remove the time step restriction based on the external gravity wave celerity, which adversely affects efficiency in low Froude number regimes. On the other hand, we showed that multilayer shallow water models can also use different numbers of layers in different mesh locations, so as to reduce the computational cost and to allow for a more efficient allocation of the degrees of freedom as well as for adaptive strategies.

Nevertheless, our previous work has an important limitation when simulating realistic flows, since the density is there assumed to be constant, as commented before. In variable density flows under the action of gravity, stratifications effects and internal gravity waves arise. Thus, the density field can have a strong effect over the dynamics of realistic coastal flows. In particular, it makes increase the vertical structure of the fluid because of the density variations (see e.g. [7, 10]). Therefore the use of multilayer models is relevant in this context to account for this vertical structure. Several multilayer models and numerical strategies have already been proposed to deal with variable density flows. In [9, 17, 6], multilayer models with variable density due to suspended sediments are introduced. In [4], the multilayer system

[2] is extended to the variable density case, where the density is constant in each layer but may be different across the layers. This model is solved using a kinetic scheme, using again an explicit time discretization. Recently, a robust second-order explicit scheme for the multilayer systems with variable density, deduced from [8], has been proposed in [13].

In the present paper, we extend the findings of [5] to the hydrostatic, variable density case in the Boussinesq regime. This work is different from the results presented in [4, 13] in several main aspects. Firstly, these papers use explicit discretizations, while we use a semi-implicit time discretization to make more efficient the multilayer method for variable density flows (for the first time to our knowledge), which allows to reduce significantly the computational cost in realistic simulations in the subcritical regime. Furthermore, in the present work the number of vertical layers is no longer constant, leading to a more flexible and efficient discretization. We also work making the Boussinesq approximation, so that the resulting system and also its numerical approximation are conceptually simpler, while still being applicable to coastal flow modelling. In addition, the proposed model and that in [13] differ from [4] in the procedure to obtain the multilayer system. Concretely, the vertical velocity and the momentum transference terms are different, and the solutions of our system yield a particular weak solution of the full Navier-Stokes system. In the present work we also study the linearization of the proposed model equations, showing how the presence of complex eigenvalues and the resulting loss of hyperbolicity are strictly related to the nontrivial vertical structure.

The paper is organized as follows: in section 2, we derive the equations defining the variable density multilayer shallow water models. In section 3, the corresponding linearized equations are derived. In section 4, the spatial semi-discretization is introduced, while the time semi-discretization approach is introduced in section 5. Results of a number of numerical experiments are reported in section 6, showing the significant efficiency gains that can be achieved by the proposed techniques. Conclusions and perspectives for future work are presented in section 7.

## 2 Variable density multilayer system

We start here from the same multilayer system as in the previous work [5] and for convenience we recall the multilayer notation introduced there. The computational domain is divided in  $N$  shallow vertical layers  $\Omega_\alpha$ ,  $\alpha = 1, \dots, N$ , where the upper and lower interfaces of layer  $\Omega_\alpha$  are  $\Gamma_{\alpha+\frac{1}{2}}$  and  $\Gamma_{\alpha-\frac{1}{2}}$ . In par-

ticular,  $\Gamma_{1/2} = b$  and  $\Gamma_{N+1/2} = \eta$  denote the topography and the free surface. As usual,  $h_\alpha$  denotes the height of the layer  $\alpha = 1, \dots, N$ , while  $h$  is the total height of the fluid, i.e.,  $h = \sum_{\alpha=1}^N h_\alpha$ . Thus, the interfaces  $\Gamma_{\alpha+1/2}$  are written  $z_{\alpha+1/2} = b + \sum_{\beta=1}^\alpha h_\beta$  and the free surface level is  $\eta = b + h$ . Finally, given a function  $f$  which is continuous at the interface  $\Gamma_{\alpha+1/2}$ , its approximation there is denoted by  $f_{\alpha+1/2}$ .

Once the notation is fixed, the multilayer system for a fluid with constant density  $\rho_0 \in \mathbb{R}^+$  is written as

$$\begin{aligned} \partial_t h_\alpha + \partial_x (h_\alpha u_\alpha) &= G_{\alpha+1/2} - G_{\alpha-1/2}, \\ \partial_t (h_\alpha u_\alpha) + \partial_x (h_\alpha u_\alpha^2) + gh_\alpha \partial_x (b+h) &= \frac{1}{\rho_0} (K_{\alpha-1/2} - K_{\alpha+1/2}) \\ &+ \frac{1}{2} G_{\alpha+1/2} (u_{\alpha+1} + u_\alpha) - \frac{1}{2} G_{\alpha-1/2} (u_\alpha + u_{\alpha-1}), \end{aligned} \quad (1)$$

for  $\alpha = 1, \dots, N$ , where  $(u_\alpha, w_\alpha) \in \mathbb{R}^2$  is the two-dimensional velocity in the layer  $\alpha$ ,  $K_{\alpha+1/2}$  account for the stresses between the layers, and  $G_{\alpha+1/2}$  is the mass transfer term between the layers  $\alpha$  and  $\alpha+1$ . These terms at the interfaces are defined through the jump condition at  $\Gamma_{\alpha+1/2}$ :

$$G_{\alpha+1/2} = \partial_t z_{\alpha+1/2} + u_{\alpha+1} \partial_x z_{\alpha+1/2} - w_{\alpha+1/2}^+ = \partial_t z_{\alpha+1/2} + u_\alpha \partial_x z_{\alpha+1/2} - w_{\alpha+1/2}^-, \quad (2)$$

see [8] for details. By defining the positive coefficient  $l_\alpha$ ,  $\alpha = 1, \dots, N$  such that  $\sum_{\alpha=1}^N l_\alpha = 1$  and  $h_\alpha = l_\alpha h$ , and using the mass conservation equation in system (1), the mass transfer terms are written as

$$G_{\alpha+1/2} = \sum_{\beta=1}^\alpha \left[ \partial_x (h l_\beta u_\beta) - l_\beta \sum_{\gamma=1}^N \partial_x (l_\gamma h u_\gamma) \right]. \quad (3)$$

Here we assume that there is no mass transfer at the bottom and the free surface, i.e.,  $G_{1/2} = G_{N+1/2} = 0$ . Then, using that  $\partial_t b = 0$ , the multilayer system can be expressed as a system with  $N+1$  equations and unknowns  $(\eta, u_1, \dots, u_N)$

$$\begin{aligned} \partial_t \eta + \partial_x \left( h \sum_{\beta=1}^N l_\beta u_\beta \right) &= 0, \\ l_\alpha h \partial_t u_\alpha + l_\alpha h u_\alpha \partial_x u_\alpha + gl_\alpha h \partial_x \eta \\ &= \frac{1}{\rho_0} (K_{\alpha-1/2} - K_{\alpha+1/2}) + G_{\alpha+1/2} \Delta \tilde{u}_{\alpha+1/2} + G_{\alpha-1/2} \Delta \tilde{u}_{\alpha-1/2}, \end{aligned} \quad (4)$$

for  $\alpha = 1, \dots, N$ , where  $\Delta\tilde{u}_{\alpha+\frac{1}{2}} = (u_{\alpha+1} - u_\alpha)/2$ . The viscous terms are

$$K_{\alpha+\frac{1}{2}} = -\nu_{\alpha+\frac{1}{2}} \mathcal{U}_{\mathcal{Z}}^H{}_{\alpha+\frac{1}{2}}, \quad (5a)$$

where  $\nu$  denotes the kinematic viscosity and  $\mathcal{U}_{\mathcal{Z}}^H{}_{\alpha+\frac{1}{2}}$  is an approximation of  $\partial_z u_\alpha$  at  $\Gamma_{\alpha+\frac{1}{2}}$ . In principle, any model can be chosen to appropriately define  $\nu_{\alpha+\frac{1}{2}}$ . The cases  $K_{\frac{1}{2}}$  and  $K_{N+\frac{1}{2}}$  have to be defined by friction coefficients at the bottom and the free surface (wind stress). Notice that a non-conservative formulation has been used, since the methods proposed in this work are most appropriate for subcritical flows.

The extension of the previous multilayer system to the case of flows with variable density is performed assuming that the Boussinesq approximation is valid [10], i.e., that the density variations are so small that their effects can be accounted for only in the computation of the pressure gradient. To this aim, we define the density in layer  $\alpha$  as  $\widetilde{\rho}_\alpha = \rho_0 + \rho'_\alpha$ , where  $\rho_0$  is a constant reference density and  $\rho'_\alpha$  is assumed to be small. More precisely, in typical geophysical applications one has  $|\rho'_\alpha/\widetilde{\rho}_\alpha| \leq O(10^{-2})$ . Under this hypothesis, the density perturbations can be accounted for only in the pressure term of the momentum equation, which must be computed by vertical integration in the multilayer framework. After some straightforward algebra, we obtain

$$\begin{aligned} \int_{\Gamma_{\alpha-\frac{1}{2}}}^{\Gamma_{\alpha+\frac{1}{2}}} \partial_x p_\alpha(z) dz &= \rho_0 g h_\alpha \partial_x \eta + g h_\alpha \partial_x \left( \sum_{\beta=\alpha+1}^N \rho'_\beta h_\beta \right) + \\ &+ g \rho'_\alpha h_\alpha \partial_x \left( b + \sum_{\beta=1}^{\alpha-1} h_\beta \right) + g \partial_x \left( \rho'_\alpha \frac{h_\alpha^2}{2} \right), \end{aligned} \quad (6)$$

where  $p_\alpha(z)$  is the pressure term of the layer  $\alpha$ . Therefore, the momentum equation in the multilayer system can be written as

$$\begin{aligned} &\rho_0 l_\alpha h \partial_t u_\alpha + \rho_0 l_\alpha h u_\alpha \partial_x u_\alpha + \rho_0 g l_\alpha h \partial_x \eta \\ &+ g l_\alpha h \partial_x \left( \frac{\rho'_\alpha h_\alpha}{2} + \sum_{\beta=\alpha+1}^N \rho'_\beta h_\beta \right) + g l_\alpha h \rho'_\alpha \partial_x \left( b + \sum_{\beta=1}^{\alpha-1} h_\beta + \frac{h_\alpha}{2} \right) \\ &= K_{\alpha-\frac{1}{2}} - K_{\alpha+\frac{1}{2}} + \rho_0 G_{\alpha+\frac{1}{2}} \Delta\tilde{u}_{\alpha+\frac{1}{2}} + \rho_0 G_{\alpha-\frac{1}{2}} \Delta\tilde{u}_{\alpha-\frac{1}{2}}. \end{aligned} \quad (7)$$

Notice that the pressure term (6) can also be rewritten as

$$\int_{\Gamma_{\alpha-1/2}}^{\Gamma_{\alpha+1/2}} \partial_x p_\alpha(z) dz = (\rho_0 + \rho'_\alpha) g h_\alpha \partial_x \eta + g h_\alpha \left( \sum_{\beta=\alpha+1}^N h_\beta \partial_x \rho'_\beta + \frac{h_\alpha \partial_x \rho'_\alpha}{2} \right) + g h_\alpha \sum_{\beta=\alpha+1}^N (\rho'_\beta - \rho'_\alpha) \partial_x h_\beta, \quad (8)$$

which can be useful if separate treatments are sought for the density perturbation gradients and the layer thickness gradients. In addition, an equation is required for the evolution of  $\rho'_\alpha$ . The mass conservation equation for the total density reads

$$\partial_t (\widetilde{\rho}_\alpha h_\alpha) + \partial_x (\widetilde{\rho}_\alpha h_\alpha u_\alpha) = \rho_0 G_{\alpha+1/2} - \rho_0 G_{\alpha-1/2} + G'_{\alpha+1/2} - G'_{\alpha-1/2},$$

where

$$G'_{\alpha+1/2} = \frac{\rho'_{\alpha+1} + \rho'_\alpha}{2} \partial_t z_{\alpha+1/2} + \frac{\rho'_{\alpha+1} u_{\alpha+1} + \rho'_\alpha u_\alpha}{2} \partial_x z_{\alpha+1/2} - \frac{\rho'_{\alpha+1} w_{\alpha+1/2}^+ + \rho'_\alpha w_{\alpha+1/2}^-}{2}.$$

Finally, by using the mass equation in (1), we obtain

$$\partial_t (\rho'_\alpha h_\alpha) + \partial_x (\rho'_\alpha h_\alpha u_\alpha) = G'_{\alpha+1/2} - G'_{\alpha-1/2}. \quad (9)$$

Since one has  $G'_{\alpha+1/2}^+ = \rho'_{\alpha+1} G_{\alpha+1/2}$ ;  $G'_{\alpha+1/2}^- = \rho'_\alpha G_{\alpha+1/2}$  and  $G'_{\alpha+1/2} = G'_{\alpha+1/2}^- = G'_{\alpha+1/2}^+$ , (see (2)) it is easy to verify that

$$G'_{\alpha+1/2} = \rho'_{\alpha+1/2} G_{\alpha+1/2}, \quad \text{with} \quad \rho'_{\alpha+1/2} = (\rho'_{\alpha+1} + \rho'_\alpha)/2.$$

Therefore, system (4)-(5) is finally re-written as

$$\begin{aligned} \partial_t \eta + \partial_x \left( h \sum_{\beta=1}^N l_\beta u_\beta \right) &= 0, \\ l_\alpha h \partial_t u_\alpha + l_\alpha h u_\alpha \partial_x u_\alpha + g l_\alpha h \partial_x \eta \\ &+ g l_\alpha h \partial_x \left( \frac{\rho_\alpha h_\alpha}{2} + \sum_{\beta=\alpha+1}^N \rho_\beta h_\beta \right) + g l_\alpha h \rho_\alpha \partial_x \left( b + \sum_{\beta=1}^{\alpha-1} h_\beta + \frac{h_\alpha}{2} \right) \\ &= \frac{1}{\rho_0} \left( K_{\alpha-1/2} - K_{\alpha+1/2} \right) + G_{\alpha+1/2} \Delta \tilde{u}_{\alpha+1/2} + G_{\alpha-1/2} \Delta \tilde{u}_{\alpha-1/2} \\ \partial_t (\rho_\alpha l_\alpha h) + \partial_x (\rho_\alpha l_\alpha h u_\alpha) &= \rho_{\alpha+1/2} G_{\alpha+1/2} - \rho_{\alpha-1/2} G_{\alpha-1/2}, \end{aligned} \quad (10)$$

for  $\alpha = 1, \dots, N$ , where we have redefined for simplicity the perturbation density as  $\rho_\alpha = \rho'_\alpha / \rho_0$ . If the reformulated pressure gradient (8) is employed, the corresponding equations

$$\partial_t \eta + \partial_x \left( h \sum_{\beta=1}^N l_\beta u_\beta \right) = 0,$$

$$\begin{aligned} l_\alpha h \partial_t u_\alpha &+ l_\alpha h u_\alpha \partial_x u_\alpha + g l_\alpha h (1 + \rho_\alpha) \partial_x \eta \\ &+ g l_\alpha h \left( \sum_{\beta=\alpha+1}^N h_\beta \partial_x \rho_\beta + \frac{h_\alpha \partial_x \rho_\alpha}{2} \right) + g l_\alpha h \sum_{\beta=\alpha+1}^N (\rho_\beta - \rho_\alpha) \partial_x h_\beta \\ &= \frac{1}{\rho_0} \left( K_{\alpha-\frac{1}{2}} - K_{\alpha+\frac{1}{2}} \right) + G_{\alpha+\frac{1}{2}} \Delta \tilde{u}_{\alpha+\frac{1}{2}} + G_{\alpha-\frac{1}{2}} \Delta \tilde{u}_{\alpha-\frac{1}{2}}, \end{aligned}$$

$$\partial_t (\rho_\alpha l_\alpha h) + \partial_x (\rho_\alpha l_\alpha h u_\alpha) = \rho_{\alpha+1/2} G_{\alpha+1/2} - \rho_{\alpha-1/2} G_{\alpha-1/2}, \quad (11)$$

are obtained for  $\alpha = 1, \dots, N$ . Notice that, as discussed [8], the above introduced equations can be regarded as a vertical discretization of the hydrostatic Navier-Stokes equations. This inevitably leads to the possibility that the proposed equations fail to constitute an hyperbolic system, since the hydrostatic (or primitive) Navier-Stokes equations are well known to lose hyperbolicity as a consequence of the hydrostatic approximation, see e.g. the classical analysis in [18].

### 3 Linear analysis

We will now derive explicitly the linearization of equations (10), in order to study the hyperbolicity of these equations at least in the linear regime and to carry out stability analyses and discuss the efficiency of time discretizations in the variable density case. We consider for simplicity the inviscid case  $\nu_{\alpha+\frac{1}{2}} = 0$  with constant number of layers  $N$  across the computational mesh. We assume that  $h = H + h'$ ,  $b = 0$  (which implies  $\eta = h$ ),  $u_\alpha = U_\alpha + u'_\alpha$ , where  $H, U_\alpha$  are constants. Concerning the density variables, on the one hand, coherently with the Boussinesq approximation, these are already small perturbations of the reference density  $\rho_0$ . On the other hand, however, the impact of stratification on the propagation of linear waves can be significant. Therefore, we will consider first the general case  $\rho_\alpha = \varrho_\alpha + \rho'_\alpha$ , allowing for different reference densities in each layer and assuming the products  $h' \varrho_\alpha$ ,  $u'_\alpha \varrho_\alpha$  to be non negligible. We will then consider the simplified case  $\varrho_\alpha = 0$ , in which possible stratification effects are disregarded.

Considering then the former situation and disregarding terms of second order in the perturbations, the following linearized equations are obtained, where the primes denoting the perturbation variables have been dropped for convenience:

$$\begin{aligned}
\partial_t h + H \sum_{\beta=1}^N l_\beta \partial_x u_\beta + \sum_{\beta=1}^N l_\beta U_\beta \partial_x h &= 0, \\
\partial_t u_\alpha + U_\alpha \partial_x u_\alpha + g \left[ 1 + \varrho_\alpha + \sum_{\beta=\alpha+1}^N l_\beta (\varrho_\beta - \varrho_\alpha) \right] \partial_x h \\
+ g \frac{l_\alpha H}{2} \partial_x \rho_\alpha + g H \sum_{\beta=\alpha+1}^N l_\beta \partial_x \rho_\beta \\
= \bar{G}_{\alpha+\frac{1}{2}} \frac{U_{\alpha+1} - U_\alpha}{2Hl_\alpha} + \bar{G}_{\alpha-\frac{1}{2}} \frac{U_\alpha - U_{\alpha-1}}{2Hl_\alpha}, \\
\partial_t \rho_\alpha + U_\alpha \partial_x \rho_\alpha = \frac{\varrho_{\alpha+1} - \varrho_\alpha}{2Hl_\alpha} \bar{G}_{\alpha+\frac{1}{2}} + \frac{\varrho_\alpha - \varrho_{\alpha-1}}{2Hl_\alpha} \bar{G}_{\alpha-\frac{1}{2}}, \tag{12}
\end{aligned}$$

where now

$$\bar{G}_{\alpha+\frac{1}{2}} = \sum_{\beta=1}^{\alpha} \left[ l_\beta H \partial_x u_\beta + l_\beta U_\beta \partial_x h - l_\beta \sum_{\gamma=1}^N l_\gamma (H \partial_x u_\gamma + U_\gamma \partial_x h) \right] \tag{13}$$

for  $\alpha = 1, \dots, N-1$  and  $\bar{G}_{\frac{1}{2}} = \bar{G}_{N+\frac{1}{2}} = 0$  as in the nonlinear case. It is important to remark here that the same equations (12) also arise from linearization of the modified system (11). For compactness, we now set, again for  $\alpha = 1, \dots, N-1$ ,

$$\begin{aligned}
\bar{U} = \sum_{\gamma=1}^N l_\gamma U_\gamma \quad \delta U_\beta = U_\beta - \bar{U} \quad \delta \bar{U}_\alpha = \sum_{\gamma=1}^{\alpha} l_\gamma \delta U_\gamma, \\
\delta_{\beta, \alpha+\frac{1}{2}} U = \frac{U_{\alpha+1} - U_\alpha}{2Hl_\beta}, \quad r_\alpha = \varrho_\alpha + \sum_{\beta=\alpha+1}^N l_\beta (\varrho_\beta - \varrho_\alpha) \tag{14}
\end{aligned}$$



and we also define the matrix

$$\begin{aligned}
M_{\alpha,\gamma} &= l_\gamma \left( 1 - \sum_{\beta=1}^{\alpha} l_\beta \right) & \text{for } \gamma \leq \alpha \\
M_{\alpha,\gamma} &= -l_\gamma \sum_{\beta=1}^{\alpha} l_\beta & \text{for } \gamma > \alpha,
\end{aligned} \tag{15}$$

so that

$$\bar{G}_{\alpha+\frac{1}{2}} = \bar{\delta U}_\alpha \partial_x h + H \sum_{\gamma=1}^N M_{\alpha,\gamma} \partial_x u_\gamma \tag{16}$$

and the momentum equations can be rewritten as

$$\begin{aligned}
&\partial_t u_\alpha + U_\alpha \partial_x u_\alpha + g(1+r_\alpha) \partial_x h + g \frac{l_\alpha H}{2} \partial_x \rho_\alpha + gH \sum_{\beta=\alpha+1}^N l_\beta \partial_x \rho_\beta \\
&= \left[ (\delta_{\alpha,\alpha+\frac{1}{2}} U) \bar{\delta U}_\alpha + (\delta_{\alpha,\alpha-\frac{1}{2}} U) \bar{\delta U}_{\alpha-1} \right] \partial_x h \\
&+ H \sum_{\gamma=1}^N \left[ (\delta_{\alpha,\alpha+\frac{1}{2}} U) M_{\alpha,\gamma} + (\delta_{\alpha,\alpha-\frac{1}{2}} U) M_{\alpha-1,\gamma} \right] \partial_x u_\gamma \\
&= -v_\alpha \partial_x h - H \sum_{\gamma=1}^N W_{\alpha,\gamma} \partial_x u_\gamma,
\end{aligned} \tag{17}$$

while the density equation reads

$$\begin{aligned}
\partial_t \rho_\alpha + U_\alpha \partial_x \rho_\alpha &= \left[ (\delta_{\alpha,\alpha+\frac{1}{2}} \varrho) \bar{\delta U}_\alpha + (\delta_{\alpha,\alpha-\frac{1}{2}} \varrho) \bar{\delta U}_{\alpha-1} \right] \partial_x h \\
&+ H \sum_{\gamma=1}^N \left[ (\delta_{\alpha,\alpha+\frac{1}{2}} \varrho) M_{\alpha,\gamma} + (\delta_{\alpha,\alpha-\frac{1}{2}} \varrho) M_{\alpha-1,\gamma} \right] \partial_x u_\gamma \\
&= -v_\alpha^\rho \partial_x h - H \sum_{\gamma=1}^N W_{\alpha,\gamma}^\rho \partial_x u_\gamma.
\end{aligned} \tag{18}$$

Setting now

$$\mathbf{q} = (h, \mathbf{u}, \boldsymbol{\rho}) = (h, u_1, \dots, u_N, \rho_1, \dots, \rho_N),$$

the previous equations can be written as

$$\partial_t \mathbf{q} + \mathbf{A} \partial_x \mathbf{q} = \mathbf{0},$$

where we have now defined

$$\mathbf{A} = \begin{bmatrix} \bar{U} & l_1 H & \dots & l_N H & 0 & \dots & 0 \\ g s_1 & U_1 + HW_{1,1} & \dots & HW_{1,N} & gl_1 H/2 & \dots & gl_N H \\ g s_2 & HW_{2,1} & \dots & HW_{2,N} & 0 & \dots & gl_N H \\ \vdots & \vdots & \ddots & \vdots & \vdots & \ddots & \vdots \\ g s_N & HW_{N,1} & \dots & U_N + HW_{N,N} & 0 & \dots & gl_N H/2 \\ v_1^\rho & HW_{1,1}^\rho & \dots & HW_{1,N}^\rho & U_1 & \dots & 0 \\ v_2^\rho & HW_{2,1}^\rho & \dots & HW_{2,N}^\rho & 0 & \dots & 0 \\ \vdots & \vdots & \ddots & \vdots & \vdots & \ddots & \vdots \\ v_N^\rho & HW_{N,1}^\rho & \dots & HW_{N,N}^\rho & 0 & \dots & U_N \end{bmatrix},$$

where now  $s_\alpha = (1 + r_\alpha + v_\alpha)$ . More compactly, this can also be rewritten as

$$\mathbf{A} = \begin{bmatrix} \bar{U} & H\mathbf{l}^T & \mathbf{0} \\ g\mathbf{s} & \mathbf{U} + H\mathbf{W} & gH\mathbf{T}\mathbf{L} \\ \mathbf{v}^\rho & H\mathbf{W}^\rho & \mathbf{U} \end{bmatrix},$$

where  $\mathbf{l} = [l_1, \dots, l_N]^T$ ,  $\mathbf{0} = [0, \dots, 0]^T$ ,  $\mathbf{s} = [s_1, \dots, s_N]^T$ ,  $\mathbf{v}^\rho = [v_1^\rho, \dots, v_N^\rho]^T$ . Note that  $\mathbf{W}$  and  $\mathbf{W}^\rho$  are the contributions corresponding to mass transfer terms multiplied by the differences of reference velocities and densities, respectively. Furthermore,  $\mathbf{L}$  denotes the diagonal matrix with elements  $l_i$  on the main diagonal,  $\mathbf{U}$  denotes the diagonal matrix with elements  $U_a$  on the main diagonal and  $\mathbf{T}$  denotes the upper triangular matrix such that

$$\mathbf{T} = \begin{bmatrix} 1/2 & 1 & \dots & 1 \\ 0 & 1/2 & \dots & 1 \\ \vdots & \vdots & \ddots & \vdots \\ 0 & 0 & \dots & 1/2 \end{bmatrix} \text{ so that } \mathbf{T}\mathbf{L} = \begin{bmatrix} l_1/2 & l_2 & \dots & l_N \\ 0 & l_2/2 & \dots & l_N \\ \vdots & \vdots & \ddots & \vdots \\ 0 & 0 & \dots & l_N/2 \end{bmatrix}.$$

The structure of  $\mathbf{A}$  is simpler if special cases are considered. For example, it can be immediately observed that, for a constant reference velocity profile, e.g.  $U_\alpha = \bar{U} = U$ , one has  $v_\alpha = 0$  and  $\mathbf{W} = \mathbf{0}$ . If the reference density values are also taken to be zero, one then has  $v_\alpha^\rho = 0$ ,  $\mathbf{W}^\rho = \mathbf{0}$  and  $\mathbf{s} = \mathbf{e} = [1, \dots, 1]^T$ , thus yielding

$$\mathbf{A} = \begin{bmatrix} U & H\mathbf{l}^T & \mathbf{0} \\ g\mathbf{e} & \mathbf{U} & gH\mathbf{T}\mathbf{L} \\ \mathbf{0} & \mathbf{0} & \mathbf{U} \end{bmatrix}.$$

In this particular case, matrix  $\mathbf{A}$  has eigenvalues  $U \pm \sqrt{gH}$  and  $U$  (with multiplicity  $2N - 1$ ), independently of the layer distribution, so that the

system is hyperbolic. If instead the reference velocity and density profiles are both constant, but  $\rho_\alpha = \rho \neq 0$ , one still has  $v_\alpha^\rho = 0$ ,  $\mathbf{W}^\rho = \mathbf{0}$ , so that

$$\mathbf{A} = \begin{bmatrix} U & H\mathbf{I}^T & \mathbf{0} \\ g\mathbf{s} & \mathbf{U} & gH\mathbf{T}\mathbf{L} \\ \mathbf{0} & \mathbf{0} & \mathbf{U} \end{bmatrix}$$

with  $s_\alpha = 1 + \rho$ ,  $\alpha = 1, \dots, N$ , so that the matrix  $\mathbf{A}$  has eigenvalues  $U \pm \sqrt{g(1 + \rho)H}$  and  $U$  (with multiplicity  $2N - 1$ ), independently of the size of the layers. On the other hand, if  $\rho_\alpha = 0$  but the reference velocity profile is not constant, it follows

$$\mathbf{A} = \begin{bmatrix} \bar{U} & H\mathbf{I}^T & \mathbf{0} \\ g\mathbf{e} & \mathbf{U} + H\mathbf{W} & gH\mathbf{T}\mathbf{L} \\ \mathbf{0} & \mathbf{0} & \mathbf{U} \end{bmatrix}.$$

The characteristic polynomial of  $\mathbf{A}$  reads then

$$\det(\mathbf{A} - \lambda\mathbf{I}) = \det(\mathbf{U} - \lambda\mathbf{I}) \det \left( \begin{bmatrix} \bar{U} - \lambda & H\mathbf{I}^T \\ g\mathbf{e} & \mathbf{U} + H\mathbf{W} - \lambda\mathbf{I} \end{bmatrix} \right). \quad (19)$$

By application of Banachiewicz-like decompositions, see e.g. [19, 20], it follows that the determinant of the last matrix is equal to

$$(\bar{U} - \lambda) \det \left( \mathbf{U} + H\mathbf{W} - \frac{\lambda - gH}{\bar{U} - \lambda} \mathbf{I} \right).$$

This implies that, if  $z$  denotes an eigenvalue of  $\mathbf{U} + H\mathbf{W}$ , the eigenvalues  $\lambda$  of  $\mathbf{A}$  must satisfy the equation

$$(z - \lambda)(\bar{U} - \lambda) - gH = 0.$$

Therefore, is it sufficient that the non symmetric part of  $\mathbf{W}$  is large enough to yield complex eigenvalues for  $\mathbf{A}$  as well. As remarked in the introduction, this should not be regarded as a deficiency of the multilayer model, but rather as a consequence of its being a convergent approximation of a three-dimensional hydrostatic flow. Let us remark that this situation is related to large deviations from the constant velocity profile, and therefore to large values of the mass transference terms  $G_{\alpha+1/2}$ . To our experience, moderate values are obtained in simulations in the hydrostatic regime. Therefore, in practice the linearized system (12) is expected to be hyperbolic.

## 4 Spatial discretization

We now consider a spatial discretization for system (10), which extends to the variable density case the finite volume approach presented in [5]. We only recall the main features of the discretization, referring to our previous paper for the full description and focusing on the novel terms coming from the variable density pressure and the evolution of the perturbations of density in each layer. It should be remarked that many other options can also be considered, such as finite difference or finite element methods.

We consider the usual finite volume description of the horizontal domain, which is subdivided into control volumes  $V_i = (x_{i-1/2}, x_{i+1/2})$ , with centers  $x_i = (x_{i+1/2} + x_{i-1/2})/2$ , for  $i = 1, \dots, M$ . The distances between  $x_i$  and  $x_{i+1}$  is denoted  $\Delta x_{i+1/2}$  and the length of the control volume is  $\Delta x_i = x_{i+1/2} - x_{i-1/2}$ . A staggered mesh is considered, where the discrete free surface and density variables  $\eta_i, \rho_i$  are defined at the centers of the control volumes,  $x_i$ , while the discrete velocities  $u_{\alpha, i+1/2}$  are defined at the interfaces,  $x_{i+1/2}$  (see figure 1).

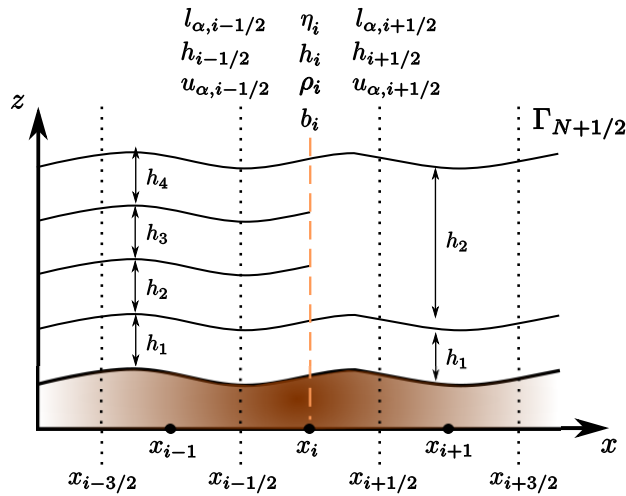


Figure 1: Sketch of the domain and of its subdivision in a variable number of layers.

As discussed in [5], the positive coefficients  $l_{\alpha, i+1/2}$  are also defined at half-integer locations, so that the number of layers  $N_{i+1/2}$  is also specified at these locations and may vary across the discrete mesh. For simplicity, the vertical mesh is assumed to be conformal, i.e., either a layer splits in several or some layers merge into a single one, and only a transition between cells with different number of layers is allowed in a 3-point stencil, i.e., it is not possible to have two consecutive transitions. These two hypothesis reduce the

complexity of the implementation, namely in the case of advection terms in the momentum equation. The number of layers at integer locations is defined as  $N_i = \max\{N_{i-\frac{1}{2}}, N_{i+\frac{1}{2}}\}$  and the discrete layer thickness coefficients at integer locations  $l_{\alpha,i}$  are taken to be equal to those at the neighbouring half-integer location with larger number of layers, that is, assuming for example  $N_{i-\frac{1}{2}} < N_{i+\frac{1}{2}}$ , we take  $l_{\alpha,i} = l_{\alpha,i+\frac{1}{2}}$ .

Given these definitions, the spatial semi-discretization reads then

$$\frac{d\eta_i}{dt} = -\frac{1}{\Delta x_i} \sum_{\beta=1}^N \left( l_{\beta,i+\frac{1}{2}} h_{i+\frac{1}{2}} u_{\beta,i+\frac{1}{2}} - l_{\beta,i-\frac{1}{2}} h_{i-\frac{1}{2}} u_{\beta,i-\frac{1}{2}} \right) \quad (20)$$

$$\begin{aligned} \frac{du_{\alpha,i+\frac{1}{2}}}{dt} &= -\frac{1}{\Delta x_{i+\frac{1}{2}}} l_{\alpha,i+\frac{1}{2}} h_{i+\frac{1}{2}} g (\eta_{i+1} - \eta_i) \\ &+ \left( \nu_{\alpha+\frac{1}{2},i+\frac{1}{2}} \frac{u_{\alpha+1,i+\frac{1}{2}} - u_{\alpha,i+\frac{1}{2}}}{l_{\alpha+\frac{1}{2},i+\frac{1}{2}} h_{i+\frac{1}{2}}} - \nu_{\alpha-\frac{1}{2},i+\frac{1}{2}} \frac{u_{\alpha,i+\frac{1}{2}} - u_{\alpha-1,i+\frac{1}{2}}}{l_{\alpha-\frac{1}{2},i+\frac{1}{2}} h_{i+\frac{1}{2}}} \right) \\ &- l_{\alpha,i+\frac{1}{2}} h_{i+\frac{1}{2}} \mathcal{A}_{\alpha,i+\frac{1}{2}}^u + \frac{1}{\Delta x_{i+\frac{1}{2}}} \left( \Delta \tilde{u}_{\alpha+\frac{1}{2},i+\frac{1}{2}} \mathcal{G}_{\alpha+\frac{1}{2},i+\frac{1}{2}} + \Delta \tilde{u}_{\alpha-\frac{1}{2},i+\frac{1}{2}} \mathcal{G}_{\alpha-\frac{1}{2},i+\frac{1}{2}} \right) \\ &- \frac{l_{\alpha,i+\frac{1}{2}} h_{i+\frac{1}{2}}}{\Delta x_{i+1/2}} g \left( \sum_{\beta=\alpha+1}^N l_{\beta,i+\frac{1}{2}} (\rho_{\beta,i+1} h_{i+1} - \rho_{\beta,i} h_i) + l_{\alpha,i+\frac{1}{2}} \frac{\rho_{\alpha,i+1} h_{i+1} - \rho_{\alpha,i} h_i}{2} \right) \\ &- \frac{l_{\alpha,i+\frac{1}{2}} h_{i+\frac{1}{2}}}{\Delta x_{i+1/2}} g \rho_{\alpha,i+\frac{1}{2}} \left( b_{i+1} - b_i + (h_{i+1} - h_i) \left( \sum_{\beta=1}^{\alpha-1} l_{\beta,i+\frac{1}{2}} + \frac{l_{\alpha,i+\frac{1}{2}}}{2} \right) \right), \quad (21) \end{aligned}$$

$$\begin{aligned} \frac{d\rho_{\alpha,i}}{dt} &= -\frac{1}{l_{\alpha,i} \Delta x_{i+\frac{1}{2}}} \left( l_{\alpha,i+\frac{1}{2}} h_{i+\frac{1}{2}} \rho_{\alpha,i+\frac{1}{2}} u_{\alpha,i+\frac{1}{2}} - l_{\alpha,i-\frac{1}{2}} h_{i-\frac{1}{2}} \rho_{\alpha,i-\frac{1}{2}} u_{\alpha,i-\frac{1}{2}} \right) \\ &+ \frac{1}{l_{\alpha,i}} \left( \rho_{\alpha+\frac{1}{2},i} G_{\alpha+\frac{1}{2},i} - \rho_{\alpha-\frac{1}{2},i} G_{\alpha-\frac{1}{2},i} \right) \quad (22) \end{aligned}$$

for  $\alpha = 1, \dots, N$ . Here  $h_{i+\frac{1}{2}}, \rho_{\alpha,i+\frac{1}{2}}, l_{\alpha,i}$  are the defined as the upwind values and  $\mathcal{A}_{\alpha,i+\frac{1}{2}}^u$  denotes the discretization of the momentum advection term, which is carried out by a first or second order upwind method. More specifically, we use the same second-order upstream based second order finite difference approximation as in [5], i.e.  $\left( u_\alpha \partial_x u_\alpha \right) \Big|_{i+1/2} = u_{\alpha,i+1/2} \partial_x u_\alpha \Big|_{i+1/2}$ ,

where

$$\partial_x u_\alpha \Big|_{i+1/2} = \begin{cases} \frac{u_{\alpha,i-\frac{3}{2}} - 4u_{\alpha,i-\frac{1}{2}} + 3u_{\alpha,i+\frac{1}{2}}}{2\Delta x_{i+\frac{1}{2}}} & \text{if } u_{\alpha,i+\frac{1}{2}} > 0, \\ -\frac{u_{\alpha,i+\frac{5}{2}} - 4u_{\alpha,i+\frac{3}{2}} + 3u_{\alpha,i+\frac{1}{2}}}{2\Delta x_{i+\frac{1}{2}}} & \text{if } u_{\alpha,i+\frac{1}{2}} < 0. \end{cases}$$

## 5 IMEX-ARK2 time discretization

This spatial discretization may be coupled with any time discretization. As in the previous work, we use an explicit third order Runge-Kutta method for the reference solutions and one of the semi-implicit scheme presented in [5], the second order IMplicit-EXplicit Additive Runge-Kutta method (IMEX-ARK2) including the terms coming to the variable density pressure terms. Moreover, we have an additional equation for the perturbations of the density, which must be discretized accordingly.

We extend here the method presented in [5] to the variable density case. To introduce IMEX-type methods, we write the ODE system as

$$\mathbf{y}' = \mathbf{f}_s(\mathbf{y}, t) + \mathbf{f}_{ns}(\mathbf{y}, t),$$

where the  $s$  and  $ns$  subscripts denote the stiff and non-stiff components of the system, respectively. In our case, we have

$$\begin{aligned} \mathbf{f}_s^0 &= -\frac{1}{\Delta x_i} \sum_{\beta=1}^N \left( l_{\beta,i+\frac{1}{2}} h_{i+\frac{1}{2}} u_{\beta,i+\frac{1}{2}} - l_{\beta,i-\frac{1}{2}} h_{i-\frac{1}{2}} u_{\beta,i-\frac{1}{2}} \right); \\ \mathbf{f}_s^{2\alpha-1} &= -\frac{1}{\Delta x_{i+\frac{1}{2}}} l_{\alpha,i+\frac{1}{2}} h_{i+\frac{1}{2}} g(\eta_{i+1} - \eta_i) \\ &\quad + \left( \nu_{\alpha+\frac{1}{2},i+\frac{1}{2}} \frac{u_{\alpha+1,i+\frac{1}{2}} - u_{\alpha,i+\frac{1}{2}}}{l_{\alpha+\frac{1}{2},i+\frac{1}{2}} h_{i+\frac{1}{2}}} - \nu_{\alpha-\frac{1}{2},i+\frac{1}{2}} \frac{u_{\alpha,i+\frac{1}{2}} - u_{\alpha-1,i+\frac{1}{2}}}{l_{\alpha-\frac{1}{2},i+\frac{1}{2}} h_{i+\frac{1}{2}}} \right), \\ \mathbf{f}_s^{2\alpha} &= -\frac{1}{l_{\alpha,i} \Delta x_{i+\frac{1}{2}}} \left( l_{\alpha,i+\frac{1}{2}} h_{i+\frac{1}{2}} \rho_{\alpha,i+\frac{1}{2}} u_{\alpha,i+\frac{1}{2}} - l_{\alpha,i-\frac{1}{2}} h_{i-\frac{1}{2}} \rho_{\alpha,i-\frac{1}{2}} u_{\alpha,i-\frac{1}{2}} \right), \end{aligned}$$

and

$$\mathbf{f}_{ns}^0 = 0;$$

$$\begin{aligned} \mathbf{f}_{ns}^{2\alpha-1} &= -l_{\alpha,i+\frac{1}{2}} h_{i+\frac{1}{2}} \mathcal{A}_{\alpha,i+\frac{1}{2}}^u + \frac{1}{\Delta x_{i+\frac{1}{2}}} \left( \Delta \tilde{u}_{\alpha+\frac{1}{2},i+\frac{1}{2}} \mathcal{G}_{\alpha+\frac{1}{2},i+\frac{1}{2}} + \Delta \tilde{u}_{\alpha-\frac{1}{2},i+\frac{1}{2}} \mathcal{G}_{\alpha-\frac{1}{2},i+\frac{1}{2}} \right) \\ &\quad - \frac{l_{\alpha,i+\frac{1}{2}} h_{i+\frac{1}{2}}}{\Delta x_{i+\frac{1}{2}}} g \left( \sum_{\beta=\alpha+1}^N l_{\beta,i+\frac{1}{2}} (\rho_{\beta,i+1} h_{i+1} - \rho_{\beta,i} h_i) + l_{\alpha,i+\frac{1}{2}} \frac{\rho_{\alpha,i+1} h_{i+1} - \rho_{\alpha,i} h_i}{2} \right) \\ &\quad - \frac{l_{\alpha,i+\frac{1}{2}} h_{i+\frac{1}{2}}}{\Delta x_{i+\frac{1}{2}}} g \rho_{\alpha,i+\frac{1}{2}} \left( b_{i+1} - b_i + (h_{i+1} - h_i) \left( \sum_{\beta=1}^{\alpha-1} l_{\beta,i+\frac{1}{2}} + \frac{l_{\alpha,i+\frac{1}{2}}}{2} \right) \right), \\ \mathbf{f}_{ns}^{2\alpha} &= \frac{1}{l_{\alpha,i}} \left( \rho_{\alpha+\frac{1}{2},i} G_{\alpha+\frac{1}{2},i} - \rho_{\alpha-\frac{1}{2},i} G_{\alpha-\frac{1}{2},i} \right), \end{aligned}$$

for  $\alpha = 1, \dots, N$ , where  $h_{i+\frac{1}{2}}, \rho_{\alpha,i+\frac{1}{2}}, l_{\alpha,i}$  are the upwind values. Note that the stiff and non-stiff parts for the extra equation are defined in order to be consistent with the continuity equation in the sense of [12].

Then, the  $s$ -stage IMEX-ARK2 method can be defined as follows. For  $l = 1, 2, 3$ :

$$\begin{aligned} \mathbf{u}^{(l)} = \mathbf{u}^n &+ \Delta t \sum_{m=1}^{l-1} \left( a_{lm} \mathbf{f}_{ns}(\mathbf{u}^{(m)}, t + c_m \Delta t) \right. \\ &\left. + \tilde{a}_{lm} \mathbf{f}_s(\mathbf{u}^{(m)}, t + c_m \Delta t) \right) + \Delta t \tilde{a}_{ll} \mathbf{f}_s(\mathbf{u}^{(l)}, t + c_l \Delta t). \end{aligned} \quad (23)$$

and the updates values  $\mathbf{u}^{n+1}$  are computed as

$$\mathbf{u}^{n+1} = \mathbf{u}^n + \Delta t \sum_{l=1}^3 b_l (\mathbf{f}_{ns}(\mathbf{u}^{(l)}, t + c_l \Delta t) + \mathbf{f}_s(\mathbf{u}^{(l)}, t + c_l \Delta t)).$$

Coefficients  $a_{lm}, \tilde{a}_{lm}, c_l$  and  $b_l$  are given to obtain a consistent method satisfying specific order and coupling conditions. We use the IMEX method proposed in [11], whose coefficients are in the Butcher tableaux, table 1 and 2 for the explicit and implicit method, respectively. The implicit part of this method matches with the TR-BDF2 scheme (see [15]), which is  $L$ -stable, and for the explicit part we have to respect the stability condition given by the Courant number  $C_{vel}$  (27). The coefficients of this part were proposed in [11].

Next, we detail the IMEX discretization for the equation of the evolution of the perturbations of the density. The mass and the momentum equations are discretized at each stage as detailed in [5], then we refer the reader to previous work for that discretized equations.

0	0	0			
$2 \mp \sqrt{2}$	$2 \mp \sqrt{2}$	$0$	$0$	$0$	$c_l$
1	$1 - (3 + 2\sqrt{2})/6$	$(3 + 2\sqrt{2})/6$	$0$	$1 \mp \frac{1}{\sqrt{2}}$	$a_{lm}$
	$\pm \frac{1}{2\sqrt{2}}$	$\pm \frac{1}{2\sqrt{2}}$			$b_l$

Table 1: *Butcher tableaux of the explicit ARK2 method*

0	0				
$2 \mp \sqrt{2}$	$1 \mp \frac{1}{\sqrt{2}}$	$1 \mp \frac{1}{\sqrt{2}}$			$\tilde{a}_{lm}$
1	$\pm \frac{1}{2\sqrt{2}}$	$\pm \frac{1}{2\sqrt{2}}$	$1 \mp \frac{1}{\sqrt{2}}$		$b_l$
	$\pm \frac{1}{2\sqrt{2}}$	$\pm \frac{1}{2\sqrt{2}}$	$1 \mp \frac{1}{\sqrt{2}}$		

Table 2: *Butcher tableaux of the implicit ARK2 method*

In order to avoid solving an extra linear system to find  $\rho_{\alpha, i+\frac{1}{2}}^{n,k}$ ,  $k = 2, 3$ , we propose a modified IMEX discretization. It consist of linearize of the density in the second and third stages of the IMEX scheme, as we detail in the following.

For the first stage, we define  $\eta_i^{n,1} = \eta_i^n$ ,  $\rho_{\alpha, i}^{n,1} = \rho_{\alpha, i}^n$ , and  $u_{\alpha, i+\frac{1}{2}}^{n,1} = u_{\alpha, i+\frac{1}{2}}^n$ , respectively. For the second stage, we have

$$\begin{aligned}
l_{\alpha, i} h_i^{n,2} \rho_{\alpha, i}^{n,2} &= l_{\alpha, i} h_i^n \rho_{\alpha, i}^n \\
&- \frac{\Delta t}{\Delta x_i} \left( l_{\alpha, i+\frac{1}{2}} h_{i+\frac{1}{2}}^n \rho_{\alpha, i+\frac{1}{2}}^{n,1} u_{\alpha, i+\frac{1}{2}}^{*,2} - l_{\alpha, i-\frac{1}{2}} h_{i-\frac{1}{2}}^n \rho_{\alpha, i-\frac{1}{2}}^{n,1} u_{\alpha, i-\frac{1}{2}}^{*,2} \right) \\
&+ a_{21} \Delta t \left( \rho_{\alpha+\frac{1}{2}, i}^{n,1} G_{\alpha+\frac{1}{2}, i}^{n,1} - \rho_{\alpha-\frac{1}{2}, i}^{n,1} G_{\alpha-\frac{1}{2}, i}^{n,1} \right),
\end{aligned}$$

where  $u_{\alpha}^{*,2} = \tilde{a}_{22} u_{\alpha}^{n,2} + \tilde{a}_{21} u_{\alpha}^{n,1}$ . Here,  $\rho_{\alpha, i+\frac{1}{2}}^{n,1}$  is computed as the upwind value depending on  $u_{\alpha}^{*,2}$ . For the third stage,

$$\begin{aligned}
l_{\alpha, i} h_i^{n,3} \rho_{\alpha, i}^{n,3} &= l_{\alpha, i} h_i^n \rho_{\alpha, i}^n \\
&- \frac{\Delta t}{\Delta x_i} \left( l_{\alpha, i+\frac{1}{2}} h_{i+\frac{1}{2}}^n \rho_{\alpha, i+\frac{1}{2}}^{n,2} u_{\alpha, i+\frac{1}{2}}^{*,3} - l_{\alpha, i-\frac{1}{2}} h_{i-\frac{1}{2}}^n \rho_{\alpha, i-\frac{1}{2}}^{n,2} u_{\alpha, i-\frac{1}{2}}^{*,3} \right) \\
&+ a_{32} \Delta t \left( \rho_{\alpha+\frac{1}{2}, i}^{n,2} G_{\alpha+\frac{1}{2}, i}^{n,2} - \rho_{\alpha-\frac{1}{2}, i}^{n,2} G_{\alpha-\frac{1}{2}, i}^{n,2} \right) \\
&- \tilde{a}_{31} \frac{\Delta t}{\Delta x_i} \left( l_{\alpha, i+\frac{1}{2}} h_{i+\frac{1}{2}}^n \rho_{\alpha, i+\frac{1}{2}}^{n,1} u_{\alpha, i+\frac{1}{2}}^{n,1} - l_{\alpha, i-\frac{1}{2}} h_{i-\frac{1}{2}}^n \rho_{\alpha, i-\frac{1}{2}}^{n,1} u_{\alpha, i-\frac{1}{2}}^{n,1} \right) \\
&+ a_{31} \Delta t \left( \rho_{\alpha+\frac{1}{2}, i}^{n,1} G_{\alpha+\frac{1}{2}, i}^{n,1} - \rho_{\alpha-\frac{1}{2}, i}^{n,1} G_{\alpha-\frac{1}{2}, i}^{n,1} \right),
\end{aligned}$$



where now  $u_\alpha^{*,3} = \tilde{a}_{32}u_\alpha^{n,3} + \tilde{a}_{31}u_\alpha^{n,2}$ , and  $\rho_{\alpha,i+\frac{1}{2}}^{n,2}$  the upwind value depending on  $u_\alpha^{*,3}$ . Finally, the assembly of the solution at time level  $n + 1$  is

$$\begin{aligned} l_{\alpha,i}h_i^{n+1}\rho_{\alpha,i}^{n+1} &= l_{\alpha,i}h_i^n\rho_{\alpha,i}^n \\ &- \frac{\Delta t}{\Delta x_i} \sum_{j=1}^3 b_j \left( l_{\alpha,i+\frac{1}{2}}h_{i+\frac{1}{2}}^n\rho_{\alpha,i+\frac{1}{2}}^{n,j}u_{\alpha,i+\frac{1}{2}}^{n,j} - l_{\alpha,i-\frac{1}{2}}h_{i-\frac{1}{2}}^n\rho_{\alpha,i-\frac{1}{2}}^{n,j}u_{\alpha,i-\frac{1}{2}}^{n,j} \right) \\ &+ \Delta t \sum_{j=1}^3 b_j \left( \rho_{\alpha+\frac{1}{2},i}^{n,j}G_{\alpha+\frac{1}{2},i}^{n,j} - \rho_{\alpha-\frac{1}{2},i}^{n,j}G_{\alpha-\frac{1}{2},i}^{n,j} \right). \end{aligned} \quad (24)$$

Notice that we obtain the consistency with the discrete continuity equation in the sense of [12] by using the values of the height at time level  $n$ ,  $h^n$ , in the advection terms. In the equations above we use the discrete transference term

$$\begin{aligned} G_{\alpha+\frac{1}{2},i}^{n,l} &= \frac{1}{\Delta x_i} \sum_{\beta=1}^{\alpha} \left( l_{\beta,i+\frac{1}{2}}h_{i+\frac{1}{2}}^n u_{\beta,i+\frac{1}{2}}^{n,l} - l_{\beta,i-\frac{1}{2}}h_{i-\frac{1}{2}}^n u_{\beta,i-\frac{1}{2}}^{n,l} \right. \\ &\quad \left. - l_{\beta,i} \sum_{\gamma=1}^N \left( l_{\gamma,i+\frac{1}{2}}h_{i+\frac{1}{2}}^n u_{\gamma,i+\frac{1}{2}}^{n,l} - l_{\gamma,i-\frac{1}{2}}h_{i-\frac{1}{2}}^n u_{\gamma,i-\frac{1}{2}}^{n,l} \right) \right), \end{aligned}$$

and  $\rho_{\alpha+\frac{1}{2},i}^{n,l}$  is the upwind value depending on the vertical velocity. To this aim, we define

$$\rho_{\alpha+1/2,i}^{n,l} = \frac{\rho_{\alpha,i}^{n,l} + \rho_{\alpha+1,i}^{n,l}}{2} - \frac{\text{sgn}\left(-G_{\alpha+\frac{1}{2},i}^{n,l}\right)}{2} \left( \rho_{\alpha+1,i}^{n,l} - \rho_{\alpha,i}^{n,l} \right), \quad (25)$$

for  $l = 1, 2, 3$ .

## 6 Numerical results

We present in this section some numerical tests in order to validate the proposed method through some academic configurations of variable density flows. Based on the linear analysis in section 3, we define a Courant number based on celerity as

$$C_{cel} = \max_{1 \leq i \leq M} \left( |\bar{u}_i| + \sqrt{(1 + \bar{\rho}_i) g h_i} \right) \frac{\Delta t}{\Delta x_i}, \quad \bar{u} = \sum_{\alpha=1}^N l_\alpha u_\alpha, \quad \bar{\rho} = \sum_{\alpha=1}^N l_\alpha \rho_\alpha, \quad (26)$$

where  $\bar{u}$ ,  $\bar{\rho}$  are the vertically averaged velocity and density perturbation corresponding to each control volume, and a Courant number based on velocity as

$$C_{vel} = \max_{1 \leq i \leq M} \left( |\bar{u}_i| + \sqrt{\bar{\rho}_i g h_i} \right) \frac{\Delta t}{\Delta x_i}, \quad \bar{u} = \sum_{\alpha=1}^N l_{\alpha} u_{\alpha}, \quad \bar{\rho} = \sum_{\alpha=1}^N l_{\alpha} \rho_{\alpha}, \quad (27)$$

Since the terms associated to the barotropic pressure gradient are treated implicitly in our approach, the resulting stability condition will be based on  $C_{vel}$  rather than  $C_{cel}$ , thus allowing for substantial computational gains.

For all the tests, we compute a reference solution with a third-order Runge-Kutta method with a fixed value  $C_{cel} = 0.1$ . That is, the time-step is adaptive, as a function of  $C_{cel}$  (26). The accuracy is measured with the following definitions:  $Err_{\eta}[l_2]$  and  $Err_{\eta}[l_{\infty}]$  denote the relative error for the free surface, and for the velocity and density fields we use

$$Err_s[l_2] = \left( \frac{\sum_{\alpha=1}^N \sum_{i=1}^M \left| s_{\alpha, i+\frac{1}{2}} - s_{\alpha, i+\frac{1}{2}}^{ref} \right|^2 \Delta x_i h_{\alpha, i}}{\sum_{\alpha=1}^N \sum_{i=1}^M \left| s_{\alpha, i+\frac{1}{2}}^{ref} \right|^2 \Delta x_i h_{\alpha, i}} \right)^{1/2}; \quad (28a)$$

$$Err_s[l_{\infty}] = \frac{\max_{\alpha} \max_i \left| s_{\alpha, i+\frac{1}{2}} - s_{\alpha, i+\frac{1}{2}}^{ref} \right|}{\max_{\alpha} \max_i \left| s_{\alpha, i+\frac{1}{2}}^{ref} \right|}, \quad (28b)$$

where  $s = \rho$  or  $s = u$ , and  $s^{ref}$  denotes the reference solution.

Note that a factor depending on the density is included in the Courant numbers (26) and (27). In these definitions,  $\bar{\rho}$  is used to obtain an approximation of the gravity wave speed associated to the density perturbation. Finally, all the computational times showed in this section have been measured on a Mac Mini with Intel<sup>®</sup>Core<sup>™</sup> i7-4578U and 16 GB of RAM.

## 6.1 Internal gravity wave

We consider here a internal gravity wave produced by a perturbation in the density field. The computational domain is  $[0, L]$ , with  $L = 2$  m. It is supposed to be closed (wall boundary conditions), with flat bottom, and the fluid at rest at initial time, when the initial height is  $\eta_0(x) = 0.3$  m everywhere. The fluid have two separate areas with densities  $\rho_1 = 1000$  kg/m<sup>3</sup> and  $\rho_2 = 1030$  kg/m<sup>3</sup>. These values are rewritten in terms of the relative perturbation as  $\rho_1 = 0$  and  $\rho_2 = 0.03$ . Thus, the initial condition for

the density is given, for  $\alpha = 1, \dots, N$ , by

$$\rho_{0,\alpha}(x) = \begin{cases} 0.03 & \text{if } z_\alpha < z_{lim} \\ 0 & \text{otherwise} \end{cases}$$

where  $z_{lim} = 0.15 + 0.04e^{-100(x-1)^2}$  and  $z_\alpha = \eta_0 \sum_{i=1}^{\beta} l_\beta$  (see figure 2). We take  $\Delta x = 0.01$  m and a non-uniform distribution of the vertical layers in order to get an accurate definition of the density perturbation. To this aim, we consider that the layers are concentrated over the central part (along the vertical direction) of the domain. Then, 54 layers are used, where four of them are in the first and last quarter of the domain, and 50 layers over the central part. Therefore, the coefficients  $l_\alpha$  are defined as

$$l_1 = l_2 = 0.125, \quad l_i = 0.01, i = 3, \dots, 52, \quad l_{53} = l_{54} = 0.125.$$

Note that this definition of the layers should be equivalent to consider 100 uniform layers. Actually, we have checked that obtained results are similar in both cases.

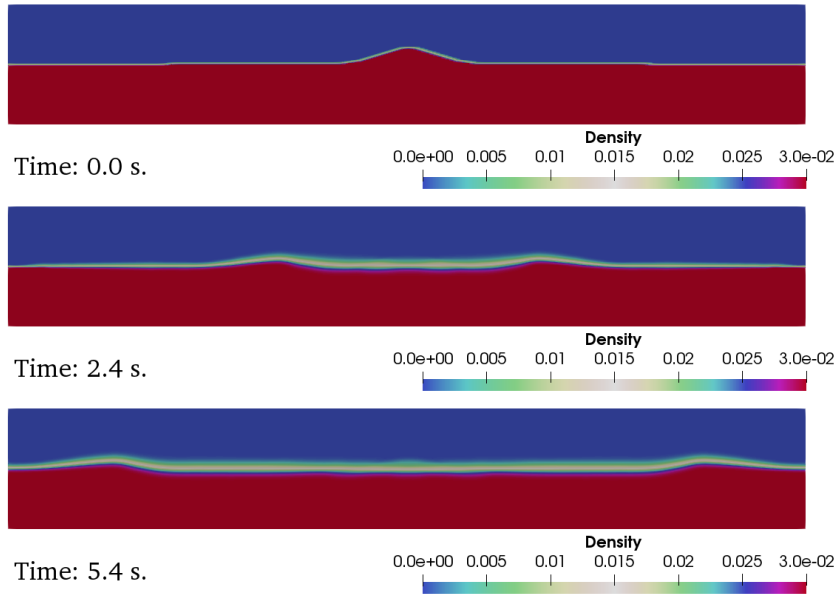


Figure 2: *Density field for different times:  $t = 0, 2.4$  and  $5.4$  s.*

In figure 2 we see the density field for the initial time, and also for  $t = 2.4, 5.4$  s. As expected, the initial density perturbation is subdivided in two internal waves, which travel in opposite directions. In this test, there is

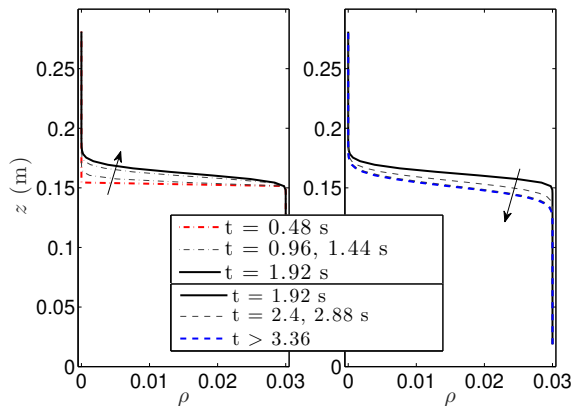


Figure 3: *Time evolution of vertical profiles of density at the point  $x = 0.745$  m.*

no significant variation of the initial height. Figure 3 shows the time evolution of the density at the point  $x = 0.745$  m. We see one of the generated waves getting through that point. Thus, the interface between the areas with different density rises and then falls. In these figures we see the numerical dissipation introduced by the vertical discretization. It could be improved by using a more accurate discretization of the equation for the density perturbation, namely for the definition of  $\rho_{\alpha+1/2}$  given by (25). Nevertheless, it is not the goal of this paper but showing how the proposed semi-implicit method is efficiently adapted to variable density flows.

Table 3 shows the relative errors and Courant numbers for this test, when comparing with the solution computed using the explicit method, at time  $t = 4.8$  s, before the perturbations arrive to the boundaries. The errors for the velocity field are greater than the ones for the density field by one order of magnitude. We have reasonable errors till Courant number  $C_{cel} = 7.0$ , which are lower than 8% and 1% for the velocity and density fields, respectively. For  $C_{cel} = 13.8$ , these errors are 10% approximately for the velocity. When a larger time step is used, the errors grow up quickly and the simulation becomes unstable for  $\Delta t \approx 0.09$ , corresponding to  $C_{vel} \approx 2.04$ .

Table 4 shows the computational times and speed-up that we obtain with the semi-implicit methods for a final time  $t_f = 10$  s. We see that with  $\Delta t = 0.04$  s, the semi-implicit method is almost 8 times faster than the explicit method with  $C_{cel} = 0.9$ , and for  $\Delta t = 0.08$  the speed-up is 16.

$\Delta t$ (s)	$C_{cel}$	$C_{vel}$	Err $_{\eta}$ [ $l_2/l_{\infty}$ ] ( $\times 10^{-4}$ )	Err $_u$ [ $l_2/l_{\infty}$ ] ( $\times 10^{-2}$ )	Err $_{\rho}$ [ $l_2/l_{\infty}$ ] ( $\times 10^{-2}$ )
0.01	1.7	0.22	0.8/2.3	2.9/1.5	0.03/0.1
0.02	3.5	0.45	0.7/1.8	7.7/6.9	0.2/1.1
0.04	7.0	0.91	2.3/5.4	7.3/15.2	0.9/6.4
0.06	10.3	1.35	1.8/3.9	10.4/27.4	1.5/10.8
0.08	13.8	1.81	1.8/3.7	10.5/21.7	1.8/14.3

Table 3: *Relative errors and Courant numbers achieved by using the IMEX-ARK2 method at  $t = 4.8$  s.*

Method	$\Delta t$ (s)	$C_{cel}$	Comput. time (s)	Speed-up
Runge-Kutta 3	-	0.1	719.3 (12 min.)	-
Runge-Kutta 3	-	0.9	83	1
IMEX-ARK2	0.01	1.7	42.1	2.0
IMEX-ARK2	0.02	3.5	20.8	4.0
IMEX-ARK2	0.04	7.0	10.8	7.7
IMEX-ARK2	0.06	10.3	7.1	11.7
IMEX-ARK2	0.08	13.8	5.2	15.9

Table 4: *Speed-ups achieved with the IMEX-ARK2 method at final time  $t_f = 10$  s.*

## 6.2 Lock exchange

Let us consider now a classical test for variable density flows, the lock exchange problem, where the fluid that is located on the right hand side of the domain have a density higher than the fluid located on the left hand side. We consider a closed domain, with  $x \in [-L/2, L/2]$ , whose length is  $L = 20$  m and  $\Delta x = 0.1$  m. In this case we take 20 uniform layers to reproduce the vertical structure of the density field.

The flow starts from the rest, with initial height  $\eta_0(x) = 0.3$  m, while the initial density is defined by the function

$$\rho_{0,\alpha}(x) = \begin{cases} 0.03 & \text{if } x > 0, \\ 0 & \text{otherwise,} \end{cases} \quad \text{for } \alpha = 1, \dots, N.$$

In this case, the discontinuous initial profile of density makes necessary to apply a flux limiter to the second-order discretization of the advection

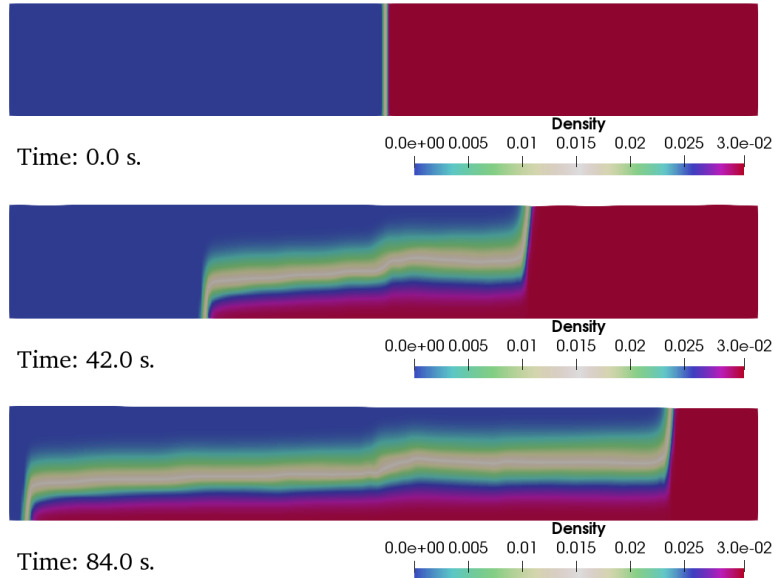


Figure 4: *Density distribution for initial time and times  $t = 42, 84$  s.*

term  $u\partial_x u$ . Otherwise, spurious oscillations appear in the simulation. Here we consider the classical *minmod* flux limiter (see e.g. [16]).

The behaviour is the expected one, qualitatively. Figure 4 shows the density field at initial time, an intermediate time ( $t = 42$  s), and the time where we measure the errors between explicit and the semi-implicit method ( $t = 84$  s).

Table 5 shows the relative errors and Courant numbers achieved, where we got a Courant number  $C_{cel} = 5.3$ . Even though the results are good enough, we see that these errors are greater than in previous test, namely for the density field. In this case, the error for the velocity and density fields are lower than 3% for  $C_{cel} = 3.5$ . However, high values of the errors are observed, in particular using the norm  $l_\infty$ , when  $C_{cel}$  are larger. It is due to the fact that the vertical structure of the fluid is stronger in this test, therefore the discretization of the mass transfer terms start playing a role and only allows to achieve Courant numbers lower than for the previous test. In addition, as commented before, since the goal of this work is to evaluate the accuracy of the proposed semi-implicit method, we have chosen a first order discretization of the equation of the density evolution (9). If one needs to reduce the error for the density and velocity, a more accurate discretization of that equation could be used.

In table 6 we see the speed-ups achieved for the semi-implicit method. We get a speed-up of 5.3 in this case.

$\Delta t$ (s)	$C_{cel}$	$C_{vel}$	Err $_{\eta}$ [ $l_2/l_{\infty}$ ] ( $\times 10^{-3}$ )	Err $_u$ [ $l_2/l_{\infty}$ ] ( $\times 10^{-2}$ )	Err $_{\rho}$ [ $l_2/l_{\infty}$ ] ( $\times 10^{-2}$ )
0.1	1.8	0.31	0.6/1.8	1.2/2.2	0.3/2.5
0.2	3.5	0.62	0.8/1.9	2.7/15.0	1.3/13.0
0.3	5.3	0.93	1.3/3.2	7.5/50.0	4.8/56.8

Table 5: *Relative errors and Courant numbers achieved by using the IMEX-ARK2 method at  $t = 84$  s.*

Method	$\Delta t$ (s)	$C_{cel}$	Comput. time (s)	Speed-up
Runge-Kutta 3	-	0.1	197.11 (3.3 min.)	-
Runge-Kutta 3	-	0.9	21.3	1
IMEX-ARK2	0.1	1.8	12.0	1.8
IMEX-ARK2	0.2	3.5	6.0	3.6
IMEX-ARK2	0.3	5.3	4.0	5.3

Table 6: *Speed-ups achieved with the IMEX-ARK2 method at final time  $t_f = 100$  s.*

We have also measured the front velocity in both, the surface and the bottom. Following [14], one could estimate that, if all the potential energy in the initial condition is transformed into kinetic energy, the theoretical velocity of the front should be  $V = \sqrt{0.25gh\rho}$ , where  $\rho$  is the density perturbation. In this case, it leads to  $V = 0.1485$  m/s. We have also numerically computed the front velocity in both the surface and the bottom. We obtain identical values for the explicit and semi-implicit methods at any time step. These velocities, measured at time  $t = 10$  s, are 0.145 m/s for the surface and 0.095 m/s for the bottom, which leads to a mean error of 19%, approximately.

### 6.3 Tidal forcing with variable density

Now, we look for a more realistic flow, simulating the mouth of a river into the sea. We consider the computational domain  $x \in [-7500, 22500]$  m, whose length is 30 km, and the variable bathymetry is given by

$$b(x) = z_0 - z_1 \tanh(\lambda(x - x_0)) + 20 e^{-(x-x_1)^2/\sigma^2},$$

with  $z_0 = -z_1 = 46$ ,  $x_0 = 7500$ ,  $x_1 = 16000$ ,  $\lambda = -1/3000$  and  $\sigma = 2000$ . This test is analogous to the one in [5] with some differences. Mainly, the

height of the bump in the bottom is 20 m. We take a smaller pick in order to ensure the subcritical regime, since an hydraulic jump due to the variable density is observed with the bottom definition in [5]. Also the height of the shallowest part of the domain is lower, in order to properly reproduce the saltwater intrusion into a river.

We consider a fluid with constant density,  $\rho_0 = 1000 \text{ kg/m}^3$ , in the whole domain at initial time. Downstream the water going into the domain have a higher density  $\rho_1 = 1030 \text{ kg/m}^3$ . To this aim, we assume that the water is at rest at initial time, and the deviation of the constant density is zero everywhere ( $\rho_{0,\alpha}(x) = 0$ ). The initial free surface is defined by  $\eta_0(x) = 100 \text{ m}$ . We consider 10 uniform vertical layers, and 500 nodes in the horizontal discretization, i.e.  $\Delta x = 60 \text{ m}$ . Now, subcritical boundary condition are imposed:

- Downstream: a tidal downstream condition  $\eta(t, L) = 100 + 3 \sin(\omega t)$  m is assumed, where  $\omega = 2\pi/43200$ . For the density, in order to avoid spurious oscillation appearing as consequence of the discontinuous boundary condition, we account for the vertical structure of the flow. In particular, we run a simulation with constant density perturbation  $\rho_\alpha(t, L) = 0.03$  for  $\alpha = 1, \dots, N$ , and after some periods of tide (when the dynamics of the flow is stabilized), the profile of the density perturbation close to the boundary is  $\rho_{\alpha,ext} = 0.03, \alpha = 1, \dots, 7$ , and

$$\rho_{8,ext} = 0.028, \quad \rho_{9,ext} = 0.025, \quad \rho_{10,ext} = 0.015.$$

Then, we consider as boundary condition the obtained profile  $\rho_\alpha(t, L) = \min(\rho_{\alpha,ext}, \rho_{\alpha,ext}t/(6 \cdot 3600))$ , that is, the density perturbation goes into the domain slowly and smoothly.

- Upstream: for the discharge, we define  $q(t, -7500) = \min(1, t/(6 \cdot 3600)) \text{ m}^2/\text{s}$ , and we impose fresh water going into the domain  $\rho_\alpha(t, -7500) = 0$ , for  $\alpha = 1, \dots, N$ .

In this case we also consider a turbulent viscosity as in [5] (we refer to previous work for details), with friction parameters  $\Delta z_r = l_1 h \text{ m}$ ,  $\Delta z_0 = 3.3 \times 10^{-5} \text{ m}$  and  $\kappa = 0.41$ . The wind drag is defined by  $C_w = 1.2 \times 10^{-6}$  and wind velocity  $u_w = 1 \text{ m/s}$ . Notice that, for the sake of simplicity, we consider this turbulence model which does not take into account the density perturbation. In realistic applications, more accurate turbulence models would have to be applied.

We simulate twelve 12-hours periods of tide, i.e., 144 h. Figure 5 shows an example of 1.5 periods of tide. The density distribution is the expected one,



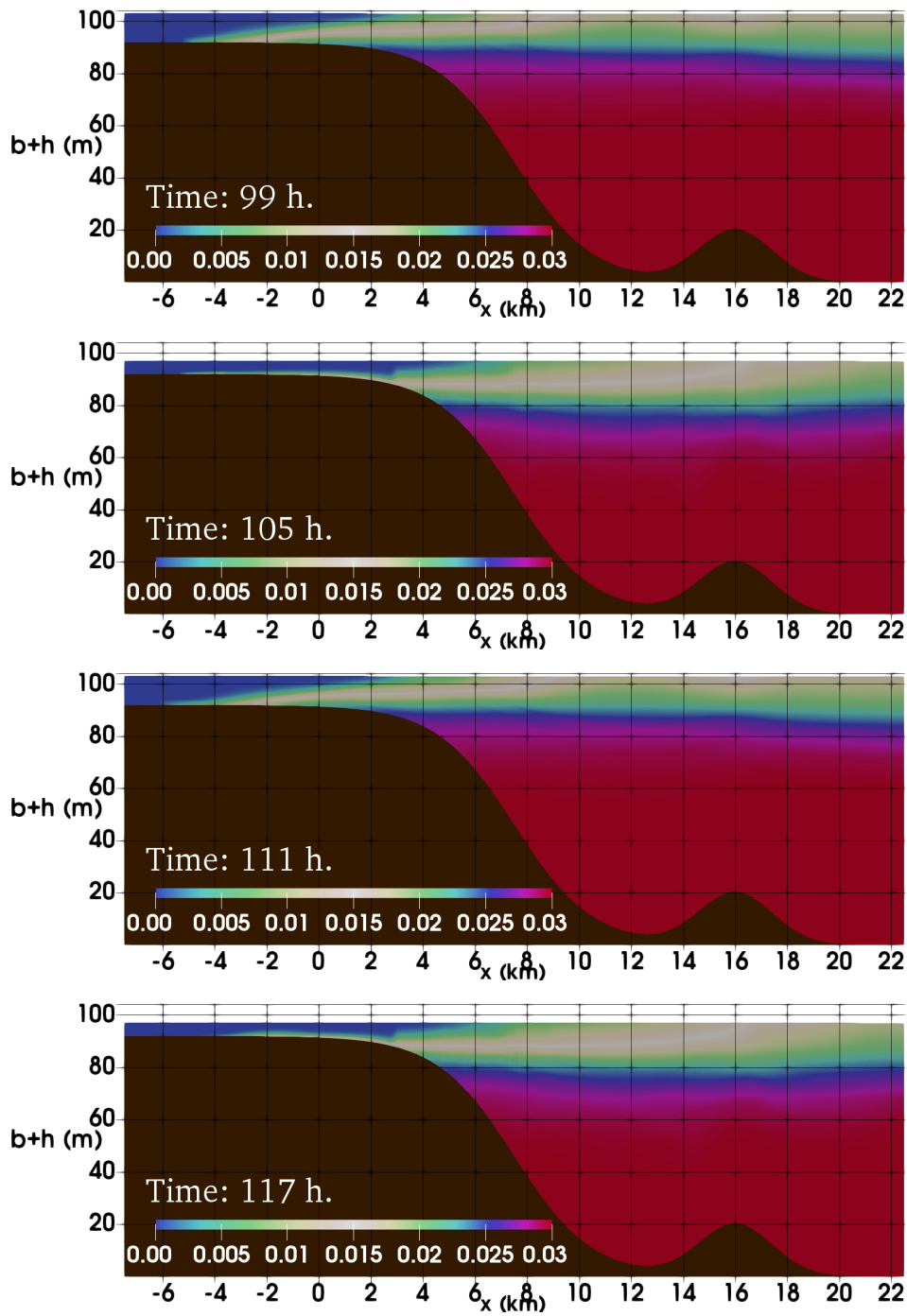


Figure 5: *Saltwater intrusion into the river at times  $t = 99, 105, 111, 117$  hours.*

the water with higher density goes to the low part of the domain, and a layer with lower density is observed in an upper layer, especially in the right-hand

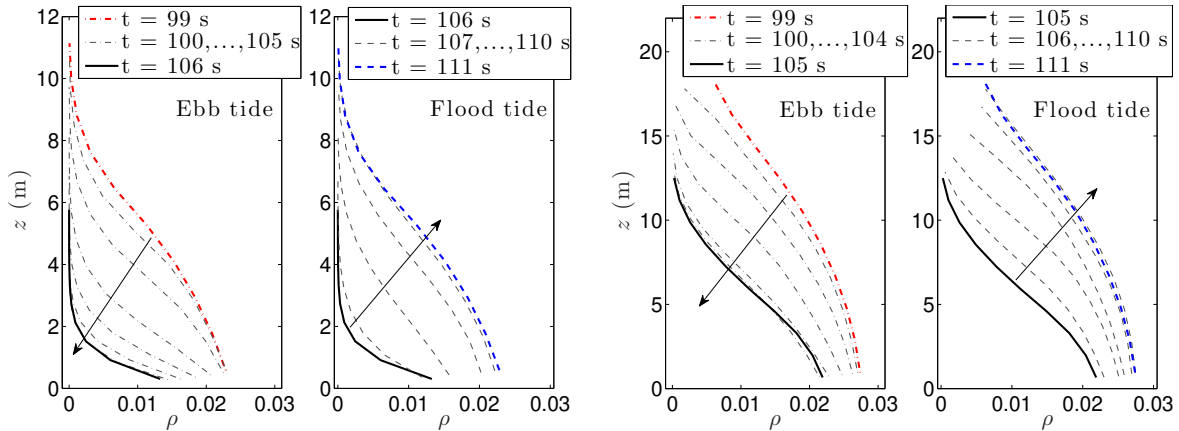


Figure 6: Time evolution of vertical profiles of density at the point  $x = 0$  km (left hand side) and  $x = 4$  km (right hand side)

side (deepest area) of the domain. The saltwater intrusion phenomenon is well reproduced, and we obtain the expected periodic behaviour. It is also observed in Figure 6, where the vertical profiles of density are shown at points  $x = 0$  km and  $x = 4$  km (mouth of the river). We see the water level falling (ebb tidal phase), and most of the water column is fresh water. Next, the water level rises (flood tidal phase) and saltwater is going into the river.

$\Delta t$ (s)	$C_{cel}$	$C_{vel}$	$Err_{\eta} [l_2/l_{\infty}]$ ( $\times 10^{-6}$ )	$Err_u [l_2/l_{\infty}]$ ( $\times 10^{-2}$ )	$Err_{\rho} [l_2/l_{\infty}]$ ( $\times 10^{-2}$ )
5	2.7	0.45	4.1/12.5	1.0/4.8	0.3/2.1
10	5.4	0.9	3.0/8.5	0.8/4.1	0.2/0.8
15	8.1	1.35	3.7/11.2	1.0/2.9	0.2/1.2
20	10.7	1.8	4.1/14.9	1.2/7.4	0.2/1.4

Table 7: Relative errors and Courant numbers achieved by using the IMEX-ARK2 method at  $t = 144$  h.

In Table 7 we see the relative errors and Courant numbers achieved at final time  $t = 144$  h. We have a Courant number  $C_{cel} = 10.7$  with  $C_{vel} = 1.8$ . The  $l_2$ -errors in the free surface position has order  $10^{-6}$ , while the errors are larger for the velocity and density fields.

Table 8 shows the speeds-up achieved with the semi-implicit method for a final time  $t = 144$  hours. The IMEX discretization is almost 5 times faster for  $\Delta t = 10$  s ( $C_{vel} = 0.9$ ), and 11 times faster for  $\Delta t = 20$  s.

In the following, we analyze the possibility of reducing the number of degrees of freedom of the multilayer system in the shallowest part of the do-

Method	$\Delta t$ (s)	$C_{cel}$	Comput. time (min)	Speed-up
Runge-Kutta 3	-	0.1	597.3 (9.95 h)	-
Runge-Kutta 3	-	0.9	68.31	1
IMEX-ARK2	5	2.7	28.95	2.4
IMEX-ARK2	10	5.4	14.52	4.7
IMEX-ARK2	15	8.1	9.69	7.0
IMEX-ARK2	20	10.7	7.25	9.4

Table 8: *Speed-ups achieved with the IMEX-ARK2 method at final time  $t_f = 144$  h.*

main. We study several configurations trying to reduce the error made, and preserving the vertical structure if needed. They are denoted hereinafter as (NVAR(n)), where (n) indicates the number of layers used in each configuration. Thus, we simplify the vertical discretization in the shallowest part of the domain ( $x < 0$  km) as follows: The vertical discretization is totally removed and a single layer is considered in the first part of the domain:

$$N = \begin{cases} 1, & l_1 = 1, & \text{if } x \leq 0; \\ 10, & l_i = 1/10, i = 1, \dots, N, & \text{otherwise.} \end{cases} \quad (\text{NVAR}(1))$$

The following configurations correspond to non-uniform distribution of the layers. Three and four layers are used in the shallowest part of the domain, increasing also the thickness of the layers close to the bottom in order to improve the vertical discretization, namely the friction effect:

$$N = \begin{cases} 3, & l_1 = l_2 = 0.2, l_3 = 0.6, & \text{if } x \leq 0; \\ 10, & l_i = 1/10, i = 1, \dots, N, & \text{otherwise,} \end{cases} \quad (\text{NVAR}(3))$$

and

$$N = \begin{cases} 4, & l_1 = l_2 = 0.2, l_3 = 0.2, l_4 = 0.4, & \text{if } x \leq 0; \\ 10, & l_i = 1/10, i = 1, \dots, N, & \text{otherwise.} \end{cases} \quad (\text{NVAR}(4))$$

For these configurations with a variable number of vertical layers, we consider the IMEX method with  $\Delta t = 10$  s in all the simulation.

Figure 7 and 8 show the vertical profiles of horizontal velocity and density at points  $x = 4$  km and  $x = 16$  km (the top of the peak) at different times. For  $x = 16$  km, which is far from the zone with reduced number of layers, the vertical profiles for configurations (NVAR(3))-(NVAR(4)) coincides with the ones using a constant number of layers. The approximation with configuration (NVAR(1)) slightly differs from these ones. For  $x = 4$  km, which is close

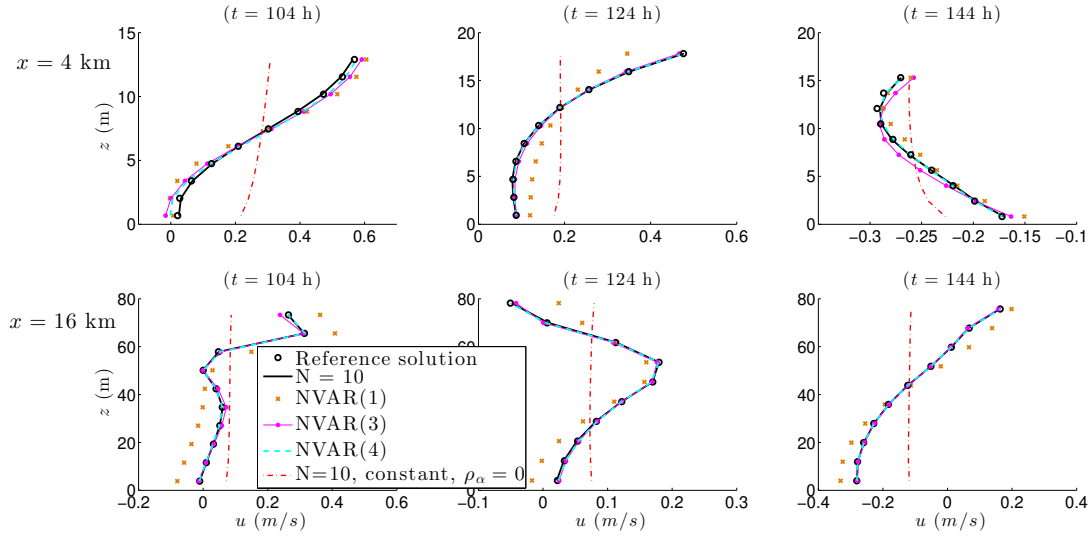


Figure 7: Vertical profiles of horizontal velocity obtained with the reference solution (black circles), and the IMEX with  $\Delta t = 10$  s, and either 10 layers in the whole domain (solid black line) or configurations (NVAR(1))-(NVAR(4)). Profiles are taken at points  $x = 4$  km and  $x = 16$  km. Dash-dotted red lines are the profiles with constant density.

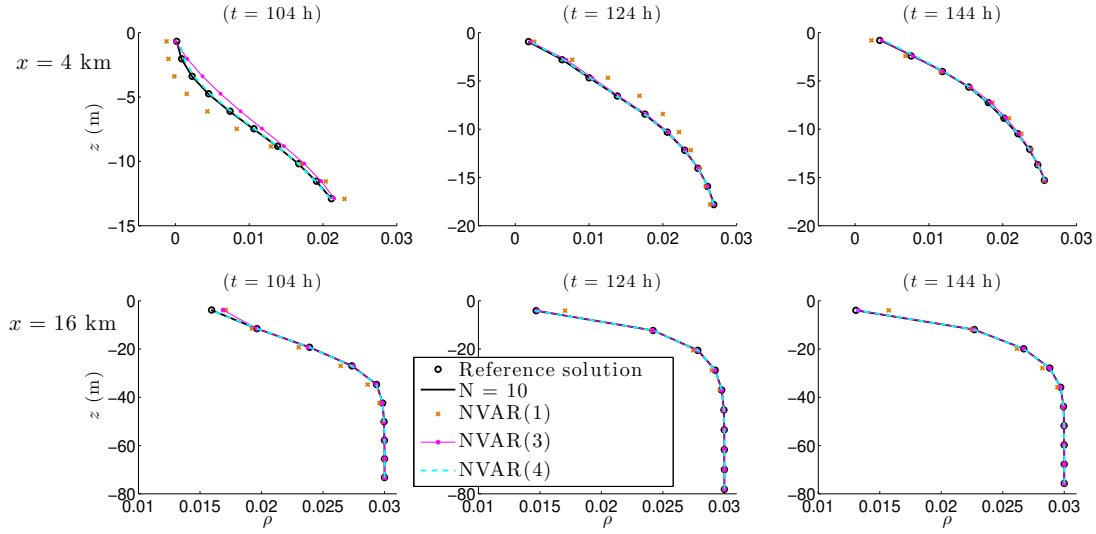


Figure 8: Vertical profiles of density obtained with the reference solution (black circles), and the IMEX with  $\Delta t = 10$  s, and either 10 layers in the whole domain (solid black line) or configurations (NVAR(1))-(NVAR(4)). Profiles are taken at points  $x = 4$  km and  $x = 16$  km.

to the zone where the transition between the area with constant and variable

number of layers occurs, we need configurations (NVAR(3))-(NVAR(4)) to reproduce the profiles with constant number of layers, although the mean variation is well reproduced by all the configurations. As conclusion, we see that configuration (NVAR(4)) notably reduce the degrees of freedom of the system and it reproduces perfectly the profiles obtained with 10 layers in the whole domain.

Figure 7 also shows the vertical profiles of velocity obtained with constant density, i.e.  $\rho_\alpha = 0$ , in the whole domain. We see that the density field notably changes the profiles of velocity, increasing the vertical structure and dynamics of the flow. This is also observed in Figure 9, where the vector velocity field is represented for the variable and constant density configurations. We see again that the vertical structure of the flow increases because of the density field and that the magnitude of the velocity is greater.

## 7 Conclusions

The numerical methods proposed in [5] for the barotropic, constant density and hydrostatic case have been extended to the variable density case in the Boussinesq regime. To this aim, a transport equation for a variable, which represents the relative deviation of a reference density, is coupled to the mass and momentum equations. Although multilayer systems with variable density have been considered previously in the literature, they have never been discretized using a semi-implicit method. An IMEX method is combined with a specific and consistent discretization of the density equation and with a multilayer description in which the number of vertical layer can vary along the computational domain. An analysis of the linearized multilayer system is presented, showing that the system is hyperbolic for moderate values of the mass transfer terms, while stronger vertical shear induces a loss of hyperbolicity, as can be expected in a three-dimensional hydrostatic flow. This analysis allows us to define appropriate Courant numbers taking into account the density field.

Some classical tests for variable density flows, as the lock exchange problem, have been performed. We have shown that the proposed semi-implicit method allows us to notably reduce the computational cost of the simulations without a significant loss of accuracy. In particular, we have shown a realistic configuration of variable density flow, which simulates the saltwater intrusion into a river. We have seen that the multilayer configuration can be adapted to complex bathymetries by changing the number of vertical layers if needed, without a loss of accuracy with respect to the simulations with constant number of vertical layers.

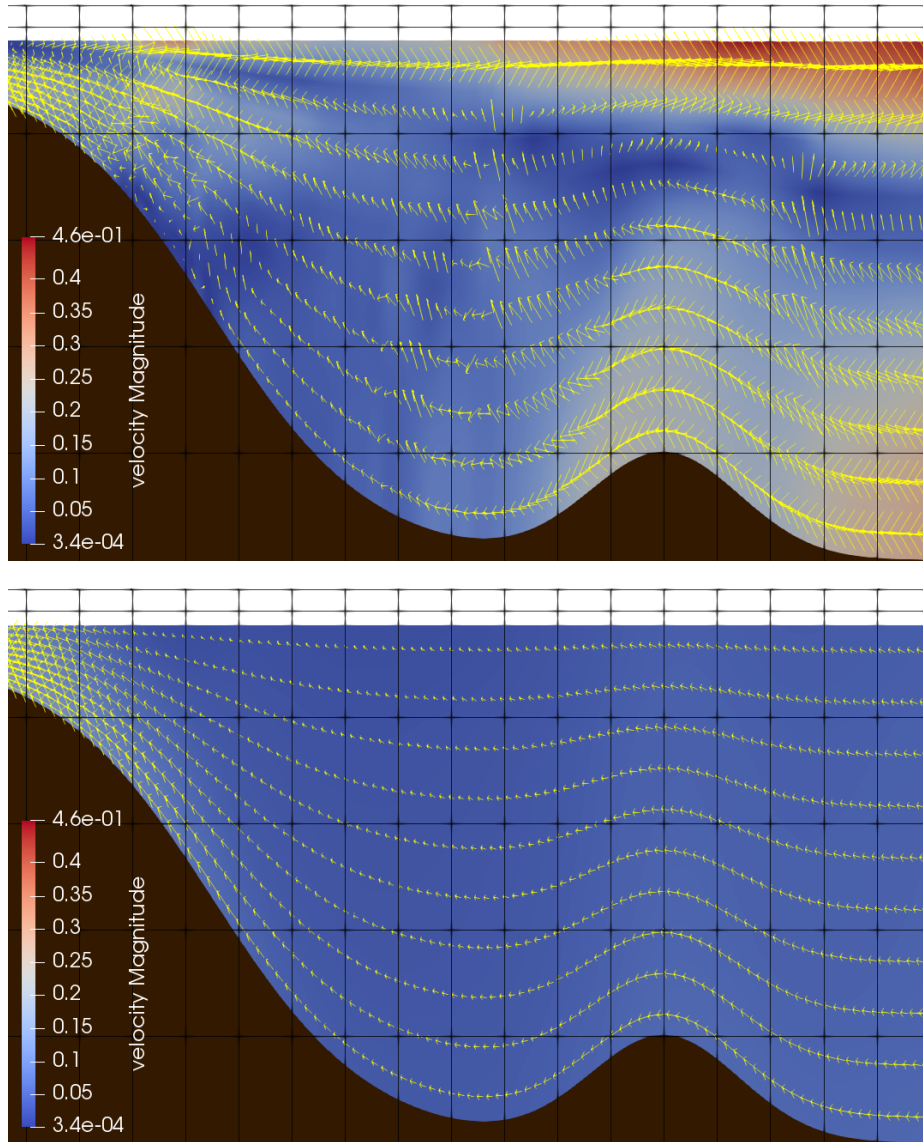


Figure 9: Vector map of the velocity field  $(u, w)$  at time  $t = 130$  h for the variable density (upper figure) and the constant density (lower figure) cases. Colors represent the magnitude of the velocity.

In future work, we will investigate even more flexible and dynamical multilayer discretizations, allowing the number of vertical layers to vary in time, as well as including more sophisticated turbulence models accounting for the non constant density field.

## Acknowledgements

This work was partially supported by the Spanish Government and FEDER through the research project RTI2018-096064-B-C22. The authors would like to thank Enrique D. Fernández-Nieto and Gladys Narbona-Reina for the interesting discussions related to this work.

## References

- [1] E. Audusse. A multilayer Saint-Venant model: derivation and numerical validation. *Discrete and Continuous Dynamical Systems Series B*, 5(2):189–214, 2005.
- [2] E. Audusse, M. Bristeau, B. Perthame, and J. Sainte-Marie. A multilayer Saint-Venant system with mass exchanges for shallow water flows. derivation and numerical validation. *ESAIM: Mathematical Modelling and Numerical Analysis*, 45:169–200, 2011.
- [3] E. Audusse, M-O. Bristeau, and A. Decoene. Numerical simulations of 3D free surface flows by a multilayer Saint-Venant model. *International Journal of Numerical Methods in Fluids*, 56(3):331–350, 2008.
- [4] E. Audusse, M-O. Bristeau, M. Pelanti, and J. Sainte-Marie. Approximation of the hydrostatic Navier-Stokes system for density stratified flows by a multilayer model: kinetic interpretation and numerical solution. *Journal of Computational Physics*, 230(9):3453–3478, 2011.
- [5] L. Bonaventura, E. D. Fernández-Nieto, J. Garres-Díaz, and G. Narbona-Reina. Multilayer shallow water models with locally variable number of layers and semi-implicit time discretization. *Journal of Computational Physics*, 364:209–234, 2018.
- [6] R. Bürger, E.D. Fernández-Nieto, and V. Osoro. A dynamic multilayer shallow water model for polydisperse sedimentation. *ESAIM: M2AN*, 53(4):1391–1432, 2019.
- [7] G.T. Csanady. Circulation in the coastal ocean. In *Advances in Geophysics*, volume 23, pages 101–183. Elsevier, 1981.
- [8] E.D. Fernández-Nieto, E.H. Koné, and T. Chacón Rebollo. A Multilayer Method for the Hydrostatic Navier-Stokes Equations: A Particular Weak Solution. *Journal of Scientific Computing*, 60(2):408–437, 2014.

- [9] E.D. Fernández-Nieto, E.H. Koné, T. Morales de Luna, and R. Bürger. A multilayer shallow water system for polydisperse sedimentation. *Journal of Computational Physics*, 238:281 – 314, 2013.
- [10] A.E. Gill. *Atmosphere-Ocean Dynamics*. Academic Press, San Diego, 1982.
- [11] F.X. Giraldo, J.F. Kelly, and E.M. Constantinescu. Implicit-explicit formulations of a three-dimensional nonhydrostatic unified model of the atmosphere (NUMA). *SIAM Journal on Scientific Computing*, 35, 2013.
- [12] E.S. Gross, L. Bonaventura, and G. Rosatti. Consistency with continuity in conservative advection schemes for free-surface models. *International Journal of Numerical Methods in Fluids*, 38:307–327, 2002.
- [13] E. Guerrero Fernández, M.J. Castro-Díaz, and T. Morales de Luna. A second-order well-balanced finite volume scheme for the multilayer shallow water model with variable density. *Mathematics*, 8(5), 2020.
- [14] J.M. Hervouet. *Hydrodynamics of Free Surface Flows*. John Wiley & Sons, Ltd, 2007.
- [15] M.E. Hosea and L.F. Shampine. Analysis and implementation of TR-BDF2. *Applied Numerical Mathematics*, 20:21–37, 1996.
- [16] R. J. LeVeque. *Finite-Volume Methods for Hyperbolic Problems*. Cambridge University Press, 2002.
- [17] T. Morales de Luna, E.D. Fernández Nieto, and M.J. Castro Díaz. Derivation of a multilayer approach to model suspended sediment transport: Application to hyperpycnal and hypopycnal plumes. *Communications in Computational Physics*, 22(5):1439–1485, 2017.
- [18] J. Olinger and A. Sundström. Theoretical and practical aspects of some initial boundary value problems in fluid dynamics. *SIAM Journal on Applied Mathematics*, 35:419–446, 1978.
- [19] J.R. Silvester. Determinants of block matrices. *The Mathematical Gazette*, 84:460–467, 2000.
- [20] Y. Tian and Y. Takaneo. More on generalized inverses of partitioned matrices with Banachiewicz–Schur forms. *Linear algebra and its applications*, 430:1641–1655, 2009.